International Journal of Precision Engineering and Manufacturing-Green Technology (2022) 9:577–585
https://doi.org/10.1007/s40684-021-00333-8

Online ISSN 2198-0810
Print ISSN 2288-6206

REGULAR PAPER

Preparation of environmentally friendly low-cost mullite porous Ceramics and the effect of Waste Glass Powder on structure and mechanical Properties

Wei Lian[1] · Yan Liu[1] · Wenjie Wang[1] · Yangtao Dong[1] · Sheng Wang[1] · Zhenying Liu[1] · Yin Liu[1,2]

Received: 8 October 2020 / Revised: 20 January 2021 / Accepted: 2 March 2021 / Published online: 19 April 2021

Abstract
Environmentally friendly low-cost porous ceramics are prepared with 98.2 wt% mining waste as the raw materials at 1180 °C. The glass powder forms liquid phase at high temperatures, promoting the densification of the materials. X-ray diffraction (XRD) results show that the formation of mullite is affected by sintering temperature and content of liquid phase. The enhancement in densification is verified by the scanning electron microscopy (SEM) analysis results. According to the evolution of pore structure, the effect of the glass powder on the structure is confirmed. The number ratio of pores of < 8 μm to those of 8 ~ 20 μm is varied from 7:2 to 2:7. The minimum apparent porosity is 31.22 %, while the maximum density and linear shrinkage are 1.75 g/cm^3 and 8.48 %, respectively. The flexural strength (three-point bending method) was increased from 7.47 MPa to 28.36 MPa, indicating that the addition of glass powder could increase mechanical properties of the porous ceramics. Therefore, solid wastes can be used as the resource to develop porous mullite ceramics.

Keywords Mullite porous ceramics · Mechanical properties · Waste disposal · Gangue

1 1. Introduction

Coal is a key energy source in developing countries. Coal gangue and slime are solid wastes produced during the coal mining and washing [1]. Their discharge and accumulation have caused serious environmental pollutions [2–5]. In order to quickly address this problem, coal gangue is used as backfill material and coal slime is used to generate electricity. However, the resources cannot be fully utilized and there are still potential environmental pollution problems, such as heavy metal pollution and fly ash [3, 6]. During the use of slime, too much ash is produced, thus resulting in serious damages to the equipment [7–9].

Mullite is a scarce ceramic material with various interesting properties in nature [10–15]. There have been reports on the preparation of mullite porous ceramics from coal gangue [16–21]. However, coal gangue only occupies 50–80 wt% of raw materials. Coal-based waste cannot be quickly consumed. Lü et al. used gangue to prepared porous mullite ceramics with high mechanical properties by in-situ synthesis method [19]. The enhanced mechanical properties result from the addition of bauxite and the high molding pressure. The use of corn starch as a pore former is not environmentally friendly. Li et al. used 80 wt% waste (coal gangue and quartz) to prepare porous ceramics with high porosity, but the mechanical properties were deteriorated [20]. In summary, the preparation of porous ceramics from waste is conducive to environmental protection and resource utilization. However, it is specifically a huge challenge to use solid wastes as the only raw materials to prepare porous ceramics without sacrificing mechanical properties.

In this work, coal gangue, coal slime, wood chips, waste glass powder and sodium carbonate were used as the raw materials to prepare mullite porous ceramics. The influence of the added amount of waste glass powder on structure and mechanical properties of the porous ceramics has been further studied. Not only the waste is effectively used, but also

✉ Yin Liu
liuyinaust@sina.com

[1] School of Materials Science and Engineering, Anhui University of Science and Technology, 232001 Huainan, Anhui, China

[2] State Key Laboratory of Mining Response and Disaster Prevention and Control in Deep Coal Mines, Anhui University of Science and Technology, 232001 Huainan, Anhui, China

Table 1 Contents and characteristics of the raw materials

Raw material	Mass percentage (wt%)	Particle size (μm)	Burning loss rate (%)
Coal cangue	62.50	< 74	6.74
Slime	26.80	< 74	57.46
Sawdust	8.90	< 180	97.80
Na_2CO_3	1.80	/	/
Glass powder	/	< 74	/

the purpose of preparing environmentally friendly materials at low cost is realized.

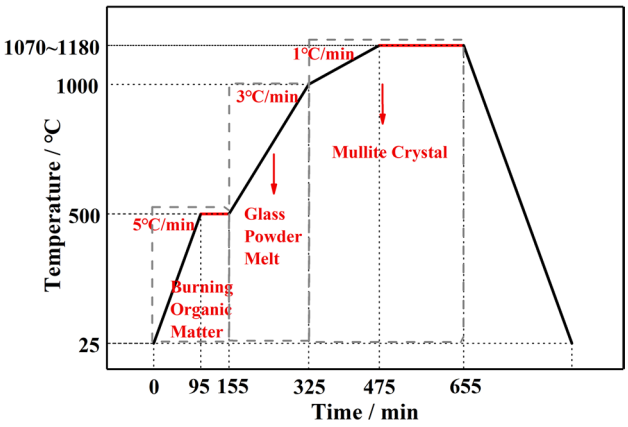

Fig. 1 Temperature profile to calcine the samples

2 2. Experimental

2.1 2.1. Samples preparation

Contents and characteristics of the raw materials are listed in Table 1. Pore structure and porosity are regulated by the burning loss rate and particle size of the raw materials. Gangue (Huainan), slime (Huainan), sawdust, flat glass powder and Na_2CO_3 (Xuzhou reagent No. 2 Factory, AR) were mixed through ball milling (XGB-04, Nanjing Boyuntong Instrument Technology Co., Ltd). 5 % deionized water is added to the mixture, so the slime has viscosity and used as a binder. Cylindrical green samples (diameter 95mm and height 3mm) and bars green samples ($4\times 4\times 40mm^3$) were prepared at a pressure of 5 MPa for 1 min. Mechanical properties and calcining properties of the porous ceramics were studied as a function of the content of the glass powder. The samples with 0%, 2%, 4% and 6% glass powder were denoted as GP0, GP2, GP4 and GP6, respectively.

2.2 2.2. Calcination

Figure 1 shows temperature profile to calcine the samples. Green samples were calcined with a box resistance furnace (SX2, Xiangtan Huafeng Instrument Manufacturing Co., Ltd, China) in oxygen atmosphere at different temperatures (1070 °C, 1100 °C, 1130 °C, 1150 °C and 1180 °C) for 3 h. Firstly, the green were samples heated from room temperature to 500 °C at a rate of 5 °C/min and kept at 500 °C for 1 h to decompose the organic phases. Then, the temperature was increased to 1000 °C at a heating rate of 3 °C/min. In this process, the glass powder melts gradually to form a liquid phase. Mechanical properties of the samples were improved due to the liquid phase can accelerate the reaction between the raw materials, while the samples were also densified. Finally, the temperature was increased to final temperatures at a heating rate of 1 °C/min and kept for 3 h. At this stage, mullite was formed, thus leading to further enhancement in mechanical properties.

2.3 2.3. Characterization

Phase compositions of the samples were studied by using X-ray diffractometer (XRD, Smart Lab, Rigaku Corporation, Japan) [22, 23]. RIR-quantitative analysis was used to calculate the phase content according to the XRD data [24]. The microstructure of the samples was observed by scanning electron microscopy (FESEM, Sigma 300, Zeiss, Germany). Archimedes method was used to measure density and apparent porosity of the samples [25, 26]. Diameters of the samples before and after calcination were used to calculate the linear shrinkage (D) by using the following Eqs. [27, 28]:

$$D = \frac{d_0 - d}{d_0} \times 100\% \tag{1}$$

where d_0 and d are the sample diameters (mm) before and after calcination, respectively.

Pore size distribution of the samples was measured by suing a pore size analysis instrument. Flexural strength of the samples was tested by using the three-point bending method with GB/T 1965–1996. The breaking force of each group is the average value of five samples broken by using universal testing machine (WDW-50, Shenzhen Kaiqiangli Test Instrument Co., Ltd, China) [29, 30]. The flexural strengths were given according to the following Eqs. [31–34]:

$$F = \frac{3lf}{2bh^2} \tag{2}$$

where F is the flexural strength (MPa), l is the span (mm) between the sample and the mold, f is the maximum stress

(N) of the samples, *b* and *h* are the width (mm) and height (mm) of the sample, respectively.

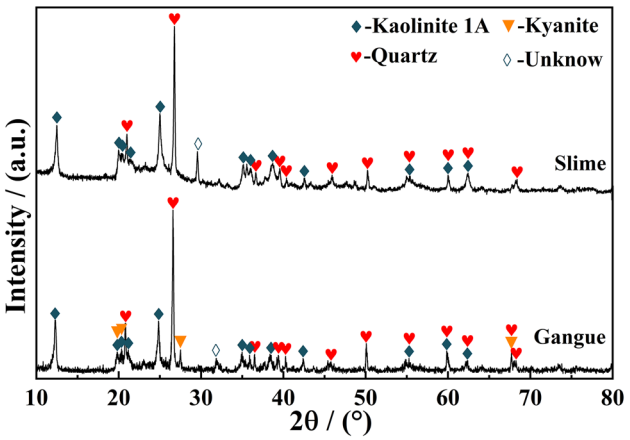

Fig. 2 XRD patterns of the raw materials

3 3. Results and discussion

3.1 3.1. Phase composition

Figure 2 shows XRD patterns of the raw materials. Kaolinite 1 A ($Al_2(Si_2O_5)(OH)_4$, PDF#80–0886), quartz (SiO_2, PDF#89-1961) and kyanite (Al_2SiO_5, PDF#83-1569) are present as the main phases of gangue. The slime also contained kaolinite 1 A ($Al_2(Si_2O_5)(OH)_4$, PDF#80–0886) and quartz (SiO_2, PDF#86-2237) as the major crystalline phases. Organic matter and minor unknown matters are observed in the slime, as demonstrated by the peaks at 20–30 ° and 29.5°. The effect of the organic and unknown matters was not studied because they were decomposed at high temperatures [14, 21, 35].

Figure 3 shows XRD patterns of the samples with different contents of glass powder calcined at different temperatures. The results show that the samples consist mainly of mullite ($Al_{4.52}Si_{1.48}O_{9.74}$, PDF#79-1457) and quartz (SiO_2, PDF#85–0930), phases are varied with the sintering temperature and the content of glass powder. Kyanite (Al_2SiO_5, PDF#83-1569) is found in samples calcined at 1070 °C, which come from coal gangue and cannot be decomposed. The kyanite crystals in GP0 calcined at 1130 °C grew up and

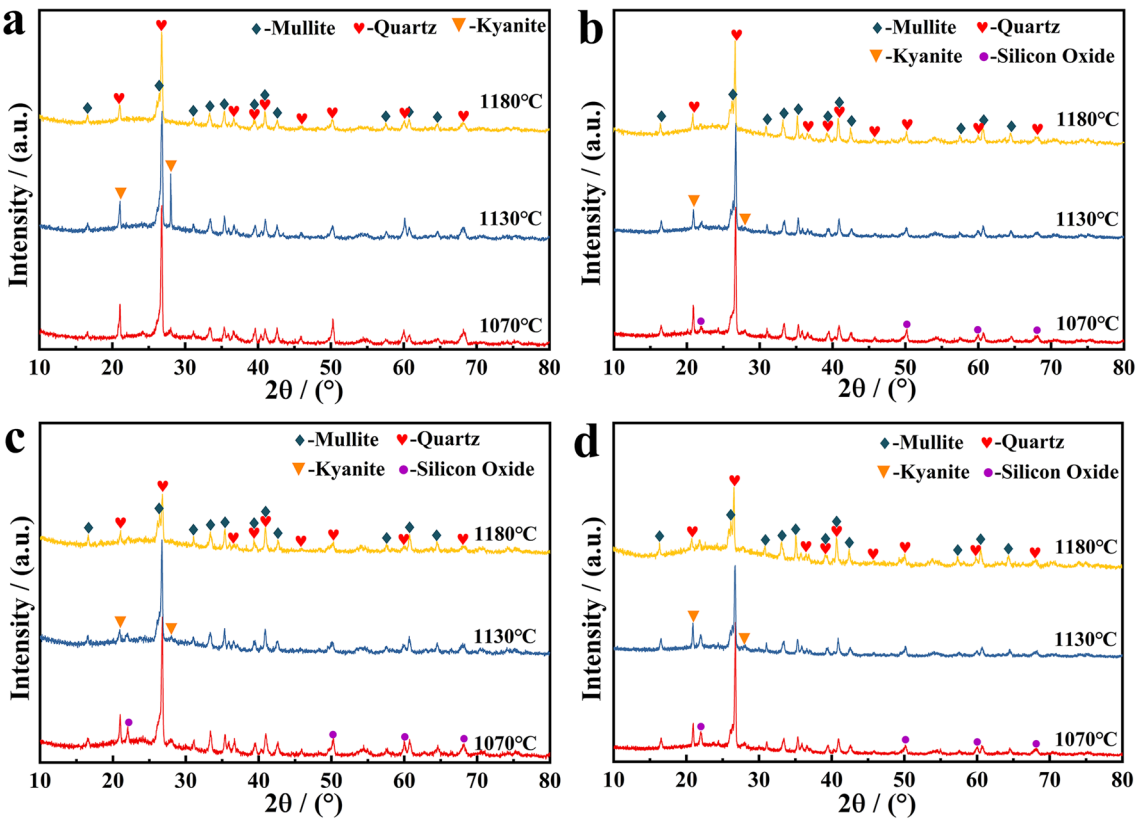

Fig. 3 XRD patterns of samples calcined at different temperatures **a** GP0, **b** GP2, **c** GP4 and **d** GP6

then was decomposed to form mullite when the temperature was rised to 1180 °C. This is consistent with the observations reported by Zhang et al. [36], but the decomposition temperature in this study is lower because of the presence of impurities in the coal gangue [35, 37, 38]. The kyanite in GP2, GP4, and GP6 decomposed at 1130 °C. The liquid phase formed at high temperatures by glass powder promote the formation of mullite, because of the increased contact between the particles. Silicon oxide (SiO_2, PDF#82-1554) in samples increases as glass powder, which confirmed that the glass powder was transformed into silicon oxide during the reaction.

Figure 4 shows XRD patterns and phase contents of the samples calcined at 1180 °C for 3 h. Mullite, quartz and silicon oxide are the main phases in the samples. As the amount of glass powder added increases, the content of silicon oxide increase, because the glass powder will transform into silicon oxide, as shown in Fig. 3. The content of mullite increase first and then decrease with increasing content of glass powder. The maximum is 64.2 % when the content of the glass powder is 4 wt%. The variation trend of quartz content is opposite to mullite. The sample with 4 wt% glass powder has a minimum content of quartz (30.3 %). Comparatively, GP4 has the largest mullite content and the smallest quartz content, which may be caused by calculation errors.

3.2 3.2. Densification

Figure 5 displays apparent porosity, density and diameter shrinkage of GP0 calcined between 1070 °C and 1180 °C[26]. The apparent porosity is more than 40.92 %, whereas the density and linear shrinkage are less than 1.50 g/cm^3 and 9.27 %, respectively. However, these characteristics change irregularly with temperature. This may be related to the incomplete reaction due to the insufficient contact of raw materials after the organic matter was burned.

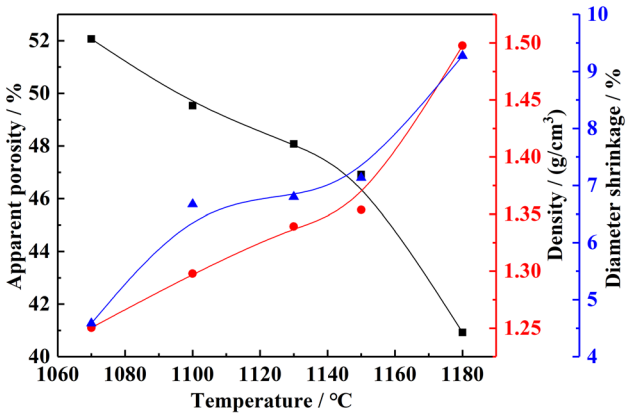

Fig. 5 Apparent porosity, density and diameter shrinkage of GP0 with calcination temperature

Figure 6 shows apparent porosity, density and linear shrinkage of GP2, GP4 and GP6 at different calcination temperatures. Compared with those of GP0, the apparent porosity, density and diameter shrinkage all have regular trend with temperature. The apparent porosity is decreased, while both the density and diameter shrinkage are increased, with increasing calcination temperature. This characteristic trend is stable up to 1180 °C. At the same temperature, the influence of glass powder on these characteristics also shows a certain variation profile. With increasing content of the glass powder, the apparent porosity decreases, while the density and diameter shrinkage increase. After calcining at 1180 °C, the apparent porosities are 34.62 %, 33.15 % and 31.22 %, for GP2, GP4 and GP6, respectively. The densities are 1.68 g/cm^3, 1.71 g/cm^3 and 1.75 g/cm^3, respectively. The corresponding diameter shrinkages are 6.93 %, 7.65 % and 8.48 %. The liquid phase formed due to the glass powder at high temperatures promoted the formation of mullite by increasing the contact between the particles of the raw materials. However, the linear shrinkage rate and bulk density of

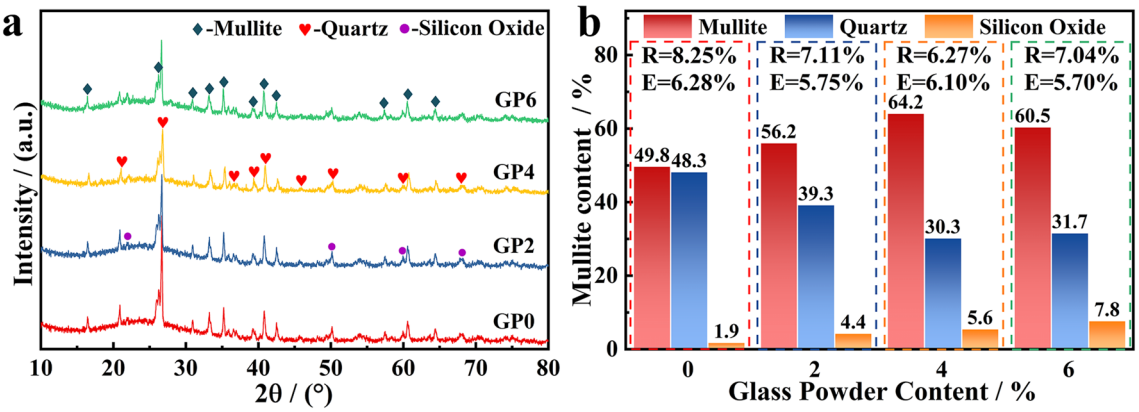

Fig. 4 XRD patterns and phase contents of the samples with different contents of glass powder after calcining at 1180 °C for 3 h

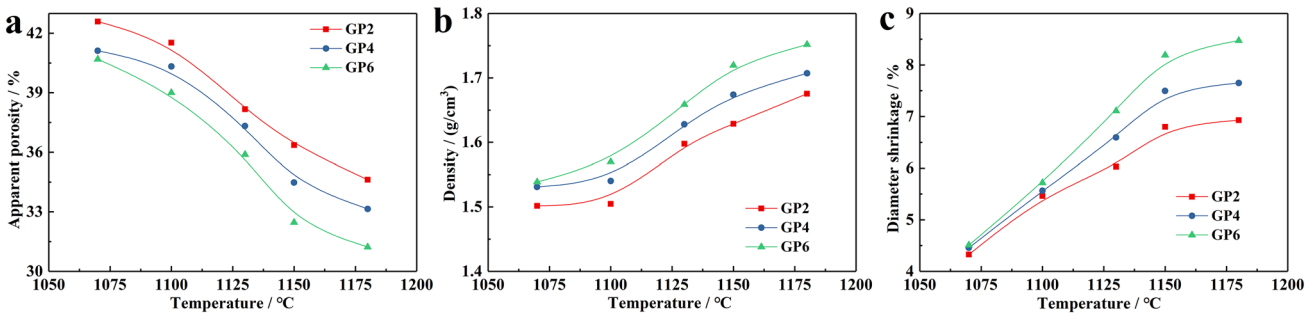

Fig. 6 Apparent porosity (**a**) density (**b**) and linear shrinkage (**c**) of GP2, GP4, GP6 with calcination temperature

the samples will increase, while the apparent porosity will decrease. The content of liquid phase in GP2 is less than those in GP4 and GP6, resulting in smaller linear shrinkage and bulk density, but the apparent porosity is higher than those of GP4 and GP6.

3.3 3.3. Microstructure

Figure 7 shows SEM images of GP0 and GP4 calcined at different temperatures. There are numerous small pores in GP0, which were formed by the accumulation of raw materials after calcining at 1070 °C. Increasing the temperature promotes the densification of GP0, but the pore size distribution is not uniform. Comparatively, GP4 calcined at 1070 °C is much compact, while the pore size and number of pores are evenly distributed. As the temperature increased, the density of GP4 is further increased. After sintering at 1180 °C, the pores can be observed clearly. This indicates that the liquid phase formed by the glass powder promotes the densification of the matrix, which is beneficial to the mechanical properties of porous ceramics.

Figure 8 shows cross-sectional SEM images of the samples with different contents of glass calcined at 1180 °C for 3 h. The GP2 sample exhibits a promising pore structure, although the distribution is not uniform, as shown in Fig. 8**a**. With the content increases of glass powder, the pore distribution becomes to be more uniform and the connectivity between the pores is improved, as shown in Fig. 8**c**. The pores are clearly observed in the enlarged image. Staggered arrangement of crystals can be seen in the pores. In addition, the unevenness of the fracture surface increases with the increase of glass powder, which is caused by crystal growth. This verified that the liquid phase derived from the glass powder promoted densification and crystal growth of the samples.

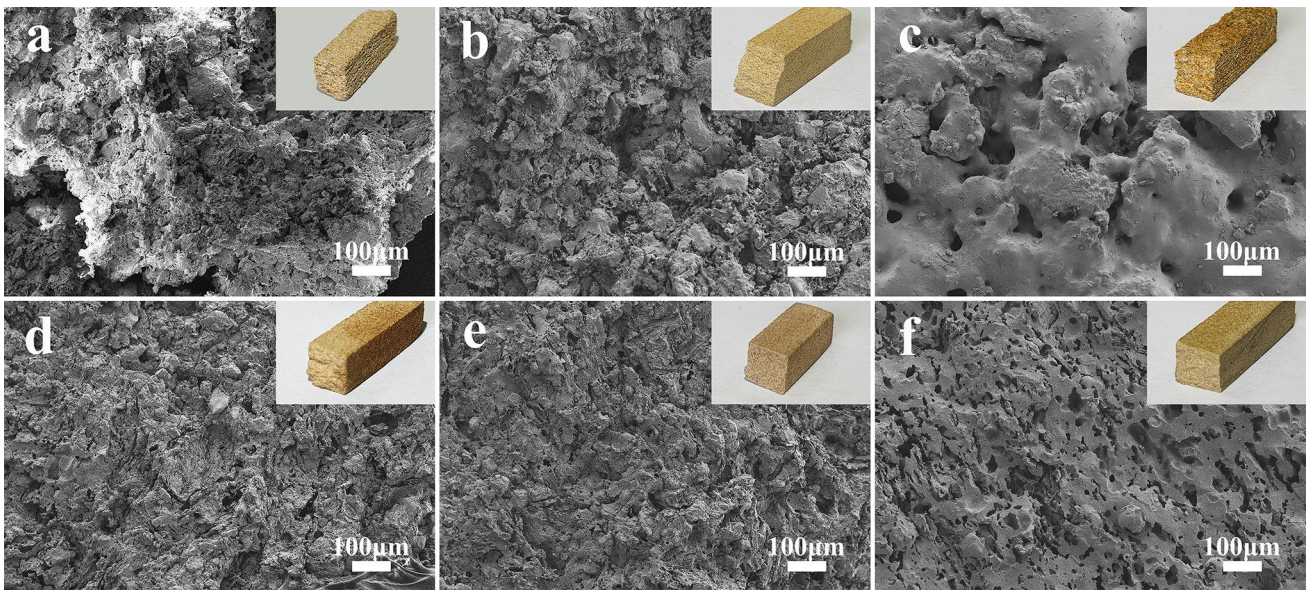

Fig. 7 SEM of representative samples **a** GP0 1070 °C, **b** GP0 1130 °C, **c** GP0 1180 °C, **d** GP4 1070 °C, **e** GP4 1130 °C and **f** GP4 1180 °C

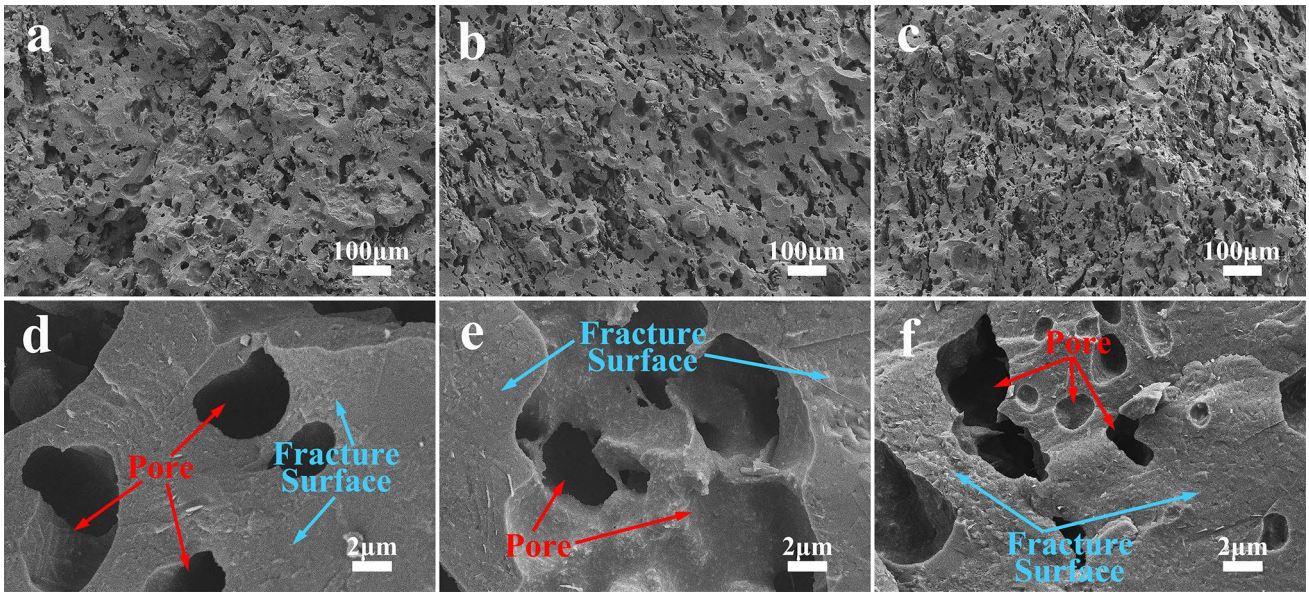

Fig. 8 Cross-sectional SEM images of the samples calcined at 1180 °C for 3 h (**a**, **d**) GP2, (**b**, **e**) GP4 and (**c**, **f**) GP6

3.4 3.4. Pore structure

Figure 9 shows pore structure characteristics of GP4 calcined at different temperatures. As presented in Fig. 9**a**, the samples contain pores with diameters of ~ 4 μm and ~ 10 μm, together with a few nanosized pores, simply because of the slime and sawdust powder have different particle sizes. However, the pore size distribution profiles of GP4 calcined at different temperatures are different. With increasing calcination temperature, the numbers of nanopore and ~ 4 μm pore are decreased, while that of ~ 10 μm pore is increased. At high temperatures, the liquid phase from the glass powder promoted densification and increased the size of the pores. As seen in Fig. 9**b**, ~ 90 % of the pores are less than 20 μm. The samples calcined at 1070 °C, 1100 °C and 1130 °C contain mainly pores of < 8 μm and a small number of 8 ~ 20 μm pores, with a ratio of 2:7. However, for the samples calcined at 1150 °C, the ratio is 7:2. All these indicate that the pore structure is changed after the addition of the glass powder. The temperature at which the pore structure changes is 1150 °C[39].

Figure 10 shows pore structure characteristics of GP2 and GP6 calcined at 1180 °C. The size and number of pores are similar with GP2 and GP6 calcined at 1180 °C. And the pore structure is similar to the GP4 sample calcined at 1150 °C. This indicates that the small difference in log differential pore volume and cumulative distribution of sample is mainly affected by the glass powder content when samples are calcined at 1180 °C. When the calcining

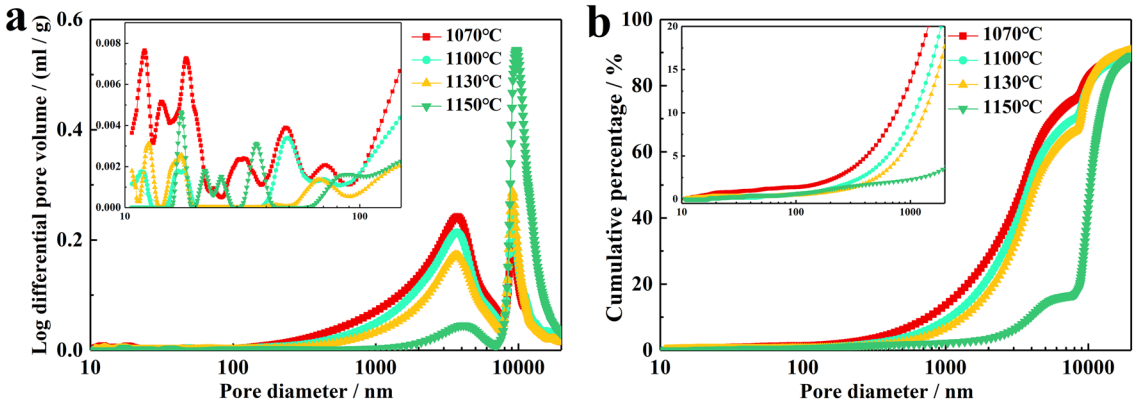

Fig. 9 Pore structure characteristics of GP4 calcined at different temperatures

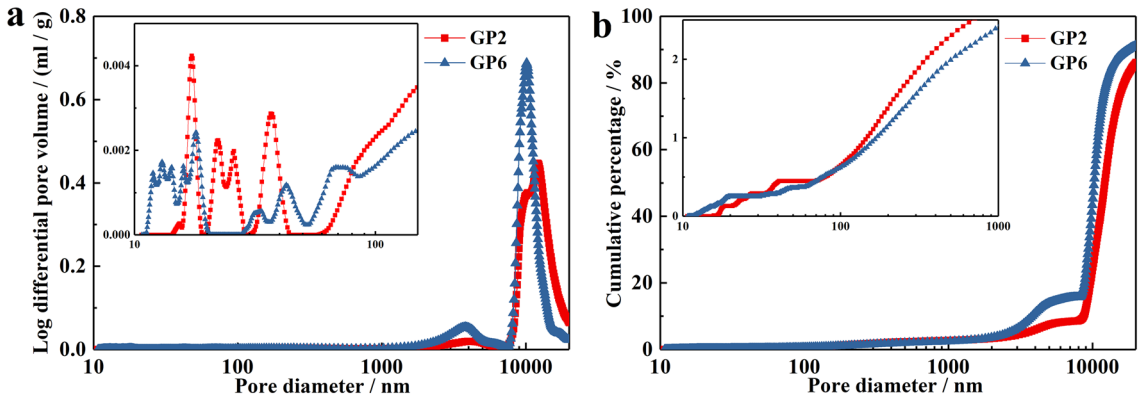

Fig. 10 Pore structure characteristics of the samples calcined at 1180 °C with different contents of glass powder

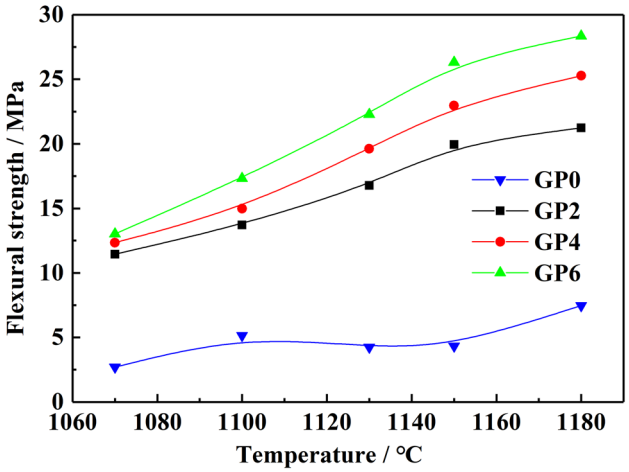

Fig. 11 Flexural strength of the samples with calcination temperature

temperature is higher than 1150 ℃, the temperature has an effect on the density (Fig. 6), but it has little effect on the pore structure.

3.5 3.5. Mechanical properties

Figure 11 shows flexural strength of the samples calcined at different temperatures. The flexural strength of GP0 is increased from 2.70 MPa to 7.47 MPa, as the sintering temperature is increased from 1070 °C to 1180 °C[34]. The fracture strengths of GP2, GP4 and GP6 calcined at 1180 °C for 3 h are 21.23 MPa, 25.27 MPa and 28.36 MPa, respectively. This suggests that the reaction and densification are insufficient at low temperatures, due to the decomposition of the organic matter. However, the presence of the liquid phase from the glass powder at high temperatures effectively enhanced the densification of the samples, thereby improving the mechanical properties.

Combining with SEM and pore structure analysis results, the flexural strength curves of GP2, GP4 and GP6 can be divided into two sections, 1070 °C − 1150 °C and 1150−1180 °C. At 1070−1150 °C, the addition of glass powder and the increase in temperature increased the density of the samples and the pore structure was adjusted. Therefore, the flexural strength increases rapidly. Above 1150 °C, the increase in flexural strength depends on the enhancement in densification, while the pore structure no longer changes.

Table 2 compares the results of this work with those reported in the open literature. Although various wastes have been used as a raw material to prepare porous ceramics, the information is not systematic. In this work, the content of waste is as high as 98.20 %, approaching an all-waste raw material utilization. Li and Ji synthesized ceramics at low temperatures with a high content of waste [20, 40]. The porous ceramic had an apparent porosity of 73 %, but the flexural strength was very low, due to the large apparent

Table 2 Comparison of this work with other ceramics

Author	Sintering temperature/°C	Apparent porosity/%	Flexural strength/MPa	Waste ratio/wt%	Ref
This work	1180	34.62	28.36	98.20	/
Li	1120	73.00	6.00	80.00	[20]
Ji	1200	1.10	51.28	60.00	[40]
Hua	1350	66.10	23.80	84.00	[41]
Guo	1500	60.71	9.63	60.00	[37]

porosity [20]. Ji used fly ash to synthesize high-density ceramics, but the flexural strength is only 51.28 MPa [40]. Hua and Guo employed high-temperature sintering to enhance the mechanical properties of high-porosity ceramics, but the effectiveness was very limited [37, 41]. Therefore, it is difficult to achieve high porosity and high flexural performance at the same time for porous ceramics prepared entirely from waste.

4 4. Conclusions

Low-cost environmentally friendly porous ceramics have been prepared with wastes as the only raw materials. The liquid phase formed due to the addition of glass powder has a positive effect on densification after sintering at 1180 °C. The number ratio of pores of < 8 μm to those of 8–20 μm was adjusted from 7:2 to 2:7. The flexural strength is increased from 7.47 MPa to 28.36 MPa. The sample calcined at 1180 °C exhibits an apparent porosity of 31.22 %, while the diameter shrinkage is less than 8.48 %, which is suitable for large-scale production. This achievement has potential economic benefits and practical values in terms of the utilization of solid wastes.

Supplementary Information The online version contains supplementary material available at https://doi.org/10.1007/s40684-021-00333-8.

Acknowledgements This work was supported by the Science and Technology Project of Anhui Province (1604a0802122 and 17030901091), the Academic Funding Project for the Top Talents of Colleges and Universities (No. gxbjZD14), Key Laboratory for Advanced Technology in Environmental Protection of Jiangsu Province (JH201840), Anhui University of science and technology 2019 Postgraduate Innovation Fund Project (2019cx2054) and National innovation and entrepreneurship training program for college students (201910361064).

Declariations

Conflict of interest On behalf of all authors, the corresponding author states that there is no conflict of interest.

References

Niu, X., Guo, S., Gao, L., Cao, Y., & Wei, X. The mercury release during thermal treatment of two coal gangues and two coal slimes under N_2 and air, Energ Fuel, (2017) 8648–8654. https://doi.org/10.1021/acs.energyfuels.7b00883.

Yang, B. Effects of coal gangue batching on raw meal burnability and working conditions of decomposing furnace, Journal of Nanjing Tech University(Natural Science Edition), (2015) 46–50.

Chao, X. U., & Kang, X. Harm and Comprehensive Utilization of Coal Gangue, Environ Sci Techno, (2010) 102–104. https://doi.org/10.3969/j.issn.1674-4829.2010.z1.034.

Qing, Z., & Guoqiang, Z. (2008). Treatment of wastewater containing Ni(II) by pyrites in coal gangue. *Environ Sci Techno, 31*, 104–105. https://doi.org/10.19672/j.cnki.1003-6504.2008.11.029.

Li, Y., Yao, Y., Liu, X., Sun, H., & Ni, W. (2013). Improvement on pozzolanic reactivity of coal gangue by integrated thermal and chemical activation. *Fuel, 109*, 527–533. https://doi.org/10.1016/j.fuel.2013.03.010.

Liu, H., & Liu, Z. (2010). Recycling utilization patterns of coal mining waste in China. *Resour Conserv Recy, 54*, 1331–1340. https://doi.org/10.1016/j.resconrec.2010.05.005.

Song, Z., Jing, C., Yao, L., Zhao, X., Ma, C., Microwave drying performance of single-particle coal slime and energy consumption analyses, Fuel Process Technol, 143 (2016) 69–78. https://doi.org/10.1016/j.fuproc.2015.11.012.

Zhou, K., Lin, Q., Hu, H., Hu, H., & Song, L. (2016). The ignition characteristics and combustion processes of the single coal slime particle under different hot-coflow conditions in N_2/O_2 atmosphere. *Energy, 136*, 173–184. https://doi.org/10.1016/j.energy.2016.02.038.

Wang, H., Liu, S., Wang, X., Shi, Y., Qin, X., & Song, C. (2017). Ignition and combustion behavior of coal slime in air. *Energ Fuel, 31*, 11439–11447. https://doi.org/10.1021/acs.energyfuels.7b01960.

Medvedovski, E. (2006). Alumina–mullite ceramics for structural applications. *Ceram Int, 32*, 369–375. https://doi.org/10.1016/j.ceramint.2005.04.001.

Hausherr, J.-M., Wagner, L., & Gorywoda, M. (2020). Fabrication of artificial defects and their effect on the mechanical properties of C/C-SiC. *J Eur Ceram Soc, 40*, 636–641. https://doi.org/10.1016/j.jeurceramsoc.2019.10.012.

Gui, K., Liu, F., Wang, G., Huang, Z., & Hu, P. (2018). Microstructural evolution and performance of carbon fiber-toughened ZrB_2 ceramics with SiC or $ZrSi_2$ additive. *J Adv Ceram, 7*, 343–351. https://doi.org/10.1007/s40145-018-0284-2.

Boussois, K., Tessier-Doyen, N., & Blanchart, P. (2013). Anisotropic kinetic of the kaolinite to mullite reaction sequence in multilayer ceramics. *J Eur Ceram Soc, 33*, 243–249. https://doi.org/10.1016/j.jeurceramsoc.2012.08.014.

De Aza, A. H., Turrillas, X., Rodriguez, M. A., Duran, T., & Pena, P. (2014). Time-resolved powder neutron diffraction study of the phase transformation sequence of kaolinite to mullite. *J Eur Ceram Soc, 34*, 1409–1421. https://doi.org/10.1016/j.jeurceramsoc.2013.10.034.

Dong, Y., Feng, X., Feng, X., Ding, Y., Liu, X., & Meng, G. (2008). Preparation of low-cost mullite ceramics from natural bauxite and industrial waste fly ash. *J Alloy Compd, 460*, 599–606. https://doi.org/10.1016/j.jallcom.2007.06.023.

Liu, L. Y., Duan, J., Li, B., Li, S., & Sang, Y. (2015). S, Preparation and Properties of Porous Mullite Refractory Aggregates Prepared Using Coal Gangue as Starting Material. *Interceram International Ceramic Review, 64*, 94–99.

Li, Z., Li, X., Tang, Y., Liu, T., Wu, T., Hao, X., & Lu, A. (2016). Sintering behaviour and characterisation of low-cost ceramic foams from coal gangue and waste quartz sand. *Adv Appl Ceram, 115*, 377–383. https://doi.org/10.1080/17436753.2016.1161692.

Qin, M., Tian, Y., Hao, H., Li, G., Zhou, Y., & Bai, P. (2020). Effects of $CaCO_3$ additive on properties and microstructure of corundum-And mullite-based ceramic proppants. *Int J Appl Ceram Tec, 17*, 1026–1032. https://doi.org/10.1111/ijac.13470.

Lu, Q., Dong, X., Zhu, Z., & Dong, Y. (2014). Environment-oriented low-cost porous mullite ceramic membrane supports fabricated from coal gangue and bauxite. *J Hazard Mater, 273*, 136–145. https://doi.org/10.1016/j.jhazmat.2014.03.026.

Li, Z., Luo, Z., Li, X., Liu, T., Guan, L., Wu, T., & Lu, A. (2015). Preparation and characterization of glass–ceramic foams with waste quartz sand and coal gangue in different proportions. *Journal of Porous Materials, 23*, 231–238. https://doi.org/10.1007/s10934-015-0074-y.

Serra, M. F., Conconi, M. S., Gauna, M. R., Suárez, G., Aglietti, E. F., & Rendtorff, N. M. (2018). Mullite ($3Al_2O_3{\cdot}2SiO_2$) ceramics

obtained by reaction sintering of rice husk ash and alumina, phase evolution, sintering and microstructure. *J Asian Ceram Soc, 4*, 61–67. https://doi.org/10.1016/j.jascer.2015.11.003.

Zhang, Z., Sha, J., Zu, Y., Dai, J., & Liu, Y. (2019). Fabrication and mechanical properties of self-toughening ZrB_2–SiC composites from in-situ reaction. *J Adv Ceram, 8*, 527–536. https://doi.org/10.1007/s40145-019-0334-4.

Zhang, W., Ma, Q., Zeng, K., Liang, S., & Mao, W. (2019). Mechanical properties and thermal stability of carbon fiber cloth reinforced sol-derived mullite composites. *J Adv Ceram, 8*, 218–227. https://doi.org/10.1007/s40145-018-0307-z.

Zhu, Z. W., Wei, Z. L., Sun, W. P., Hou, J., He, B. H., & Dong, Y. C. (2016). Cost-effective utilization of mineral-based raw materials for preparation of porous mullite ceramic membranes via in-situ reaction method. *Appl Clay Sci, 120*, 135–141. https://doi.org/10.1016/j.clay.2015.11.020.

Liao, N., Jia, D., Yang, Z., & Zhou, Y. (2019). Enhanced mechanical properties and thermal shock resistance of Si_2BC_3N ceramics with SiC coated MWCNTs. *J Adv Ceram, 8*, 121–132. https://doi.org/10.1007/s40145-018-0300-6.

Lee, J.-C., & Ahn, S.-H. (2018). Bulk density measurement of porous functionally graded materials. *International Journal of Precision Engineering and Manufacturing, 19*, 31–37. https://doi.org/10.1007/s12541-018-0004-4.

Liu, P., Li, Z., Xiao, P., Luo, H., & Jiang, T. (2018). Microstructure and mechanical properties of in-situ grown mullite toughened 3Y-TZP zirconia ceramics fabricated by gelcasting. *Ceram Int, 44*, 1394–1403. https://doi.org/10.1016/j.ceramint.2017.09.151.

Xu, X. H., Lao, X. B., Wu, J. F., Xu, X. Y., Zhang, Y. X., & Li, K. (2016). In-situ synthesis of SiCw/Al_2O_3 composite honeycomb ceramics by aluminium-assisted carbothermal reduction of coal series kaolin. *Appl Clay Sci, 126*, 122–131. https://doi.org/10.1016/j.clay.2016.03.008.

Choi, Y.-J., Song, M.-S., Yoo, Y.-J., & Lee, J.-S. (2014). Fracture Analysis for Ceramic Disk with Semi-Elliptical Crack and Pore. *International Journal of Precision Engineering and Manufacturing, 15*, 433–438. https://doi.org/10.1007/s12541-014-0354-5.

Sung, J.-W., Kim, K.-H., & Kang, M.-C. (2016). Effects of graphene nanoplatelet contents on material and machining properties of GNP-dispersed Al_2O_3 ceramics for micro-electric discharge machining. *International Journal of Precision Engineering and Manufacturing-Green Technology, 3*, 247–252. https://doi.org/10.1007/s40684-016-0032-4.

Dong, Y., Zhou, J., Lin, B., Wang, Y., Wang, S., Miao, L., Lang, Y., Liu, X., & Meng, G. (2009). Reaction-calcined porous mineral-based mullite ceramic membrane supports made from recycled materials. *J Hazard Mater, 172*, 180–186. https://doi.org/10.1016/j.jhazmat.2009.06.148.

Jing, Q., Bao, J., Ruan, F., Song, X., An, S., Zhang, Y., Tian, Z., Xie, M., & Gao, J. (2019). The effect of YF_3 on the mechanical properties and low-temperature degradation of 3Y-TZP ceramics. *Ceram Int, 45*, 24212–24220. https://doi.org/10.1016/j.ceramint.2019.08.130.

Cheng, Z., Ye, F., Liu, Y., Qiao, T., Li, J., Qin, H., Cheng, L., & Zhang, L. (2019). Mechanical and dielectric properties of porous and wave-transparent Si_3N_4-Si_3N_4 composite ceramics fabricated by 3D printing combined with chemical vapor infiltration. *J Adv Ceram, 8*, 399–407. https://doi.org/10.1007/s40145-019-0322-8.

Guo, H. S., Li, W. F., & Ye, F. B. (2016). Low-cost porous mullite ceramic membrane supports fabricated from kyanite by casting and reaction sintering. *Ceram Int, 42*, 4819–4826. https://doi.org/10.1016/j.ceramint.2015.11.167.

Guo, H., & Li, W. (2018). Effects of Al_2O_3 crystal types on morphologies, formation mechanisms of mullite and properties of porous mullite ceramics based on kyanite. *J Eur Ceram Soc, 38*, 679–686. https://doi.org/10.1016/j.jeurceramsoc.2017.09.003.

Jinhua, Z., Hongdan, W., Suxin, Z., Jishun, Y., & Shuren, H. (2013). Preparation of mullite whiskers and their enhancement effect on ceramic matrix composites. *Journal of Wuhan University of Technology-Mater, 28*, 271–275. https://doi.org/10.1007/s11595-013-0715-4.

Guo, H., Li, W., & Ye, F. (2016). Low-cost porous mullite ceramic membrane supports fabricated from kyanite by casting and reaction sintering. *Ceram Int, 42*, 4819–4826. https://doi.org/10.1016/j.ceramint.2015.11.167.

Deutou, J. G. N., Mohamed, H., Nzeukou, N. A., Kamseu, E., Melo, U. C., Beda, T., & Leonelli, C. (2016). The role of kyanite in the improvement in the crystallization and densification of the high strength mullite matrix Phase evolution and sintering behaviour. *J Therml Anal Calorim, 126*, 1211–1222. https://doi.org/10.1007/s10973-016-5686-1.

Lee, D. G., Kim, S.-H., Kim, S., Yu, J. H., & Cho, S. W. (2019). Prediction of Material Properties of Ceramic Composite Material by Porous Structure and Porosity Using the Finite Element Method. *International Journal of Precision Engineering and Manufacturing, 20*, 805–814. https://doi.org/10.1007/s12541-019-00127-8.

Ji, R., Zhang, Z., Yan, C., Zhu, M., & Li, Z. (2016). Preparation of novel ceramic tiles with high Al_2O_3 content derived from coal fly ash. *Constr Build Mater, 114*, 888–895. https://doi.org/10.1016/j.conbuildmat.2016.04.014.

Hua, K., Shui, A., Xu, L., Zhao, K., Zhou, Q., & Xi, X. (2016). Fabrication and characterization of anorthite–mullite–corundum porous ceramics from construction waste. *Ceram Int, 42*, 6080–6087. https://doi.org/10.1016/j.ceramint.2015.12.165.